ACS APPLIED MATERIALS & INTERFACES

Letter

www.acsami.org

Photocatalytic Water Splitting under Visible Light by Mixed-Valence Sn_3O_4

Maidhily Manikandan,[†,‡] Toyokazu Tanabe,[†] Peng Li,[†] Shigenori Ueda,[§] Gubbala V. Ramesh,[†] Rajesh Kodiyath,[†] Junjie Wang,[†] Toru Hara,[†] Arivuoli Dakshanamoorthy,[‡] Shinsuke Ishihara,[#] Katsuhiko Ariga,[#,⊥] Jinhua Ye,[†,#] Naoto Umezawa,*[,†,⊥] and Hideki Abe*[,†,⊥]

[†]National Institute for Materials Science, 1-1 Namiki, Tsukuba, Ibaraki 305-0044, Japan

[‡]Crystal Growth Centre, Anna University, Chennai, Tamil Nadu 600-025, India

[§]Synchrotron X-ray Station at SPring-8, National Institute for Materials Science, 1-1-1 Kouto, Sayo, Hyogo 679-5148, Japan

[#]International Center for Material Nanoarchitectonics, National Institute for Materials Science, 1-1 Namiki, Tsukuba, Ibaraki 305-0044, Japan

[⊥]Precursory Research for Embryonic Science and Technology (PRESTO) and Core Research for Evolutional Science and Technology (CREST), Japan Science and Technology Agency (JST), 4-1-8 Honcho, Kawaguchi, Saitama 332-0012, Japan

Supporting Information

ABSTRACT: A mixed-valence tin oxide, $(Sn^{2+})_2(Sn^{4+})O_4$, was synthesized via a hydrothermal route. The Sn_3O_4 material consisted of highly crystalline {110} flexes. The Sn_3O_4 material, when pure platinum (Pt) was used as a co-catalyst, significantly catalyzed water-splitting in aqueous solution under illumination of visible light ($\lambda > 400$ nm), whereas neither $Sn^{2+}O$ nor $Sn^{4+}O_2$ was active toward the reaction. Theoretical calculations have demonstrated that the co-existence of Sn^{2+} and Sn^{4+} in Sn_3O_4 leads to a desirable band structure for photocatalytic hydrogen evolution from water solution. Sn_3O_4 has great potential as an abundant, cheap, and environmentally benign solar-energy conversion catalyst.

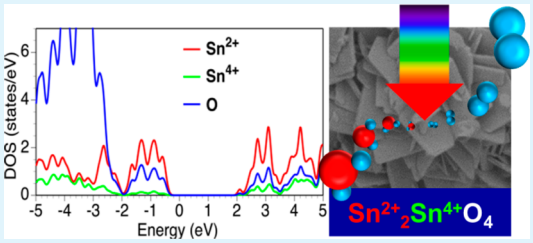

KEYWORDS: *photocatalyst, water splitting, visible light, tin oxide, mixed valence*

INTRODUCTION

The increasing interest in renewable energies has highlighted the centrality of sustainable energy-conversion technologies including photocatalytic water splitting.[1−6] In particular, catalytic water splitting in visible light by visible-light-sensitive photocatalysts is of confocal interest because this will realize efficient conversion of the solar energy to hydrogen fuels for sustainable energy managements.[7,8] Metal-doped $SrTiO_3$ (dopants: Ta, Rh or Ni) and metal oxides, $RbPb_2Nb_3O_{10}$ and $SnNb_2O_6$, can catalyze water splitting under illumination of visible light in the presence of sacrificial agents.[9−12] Oxynitrides of transition metals or lanthanides such as TaON and $LaTiO_2N$ can promote hydrogen evolution from water solution in visible light.[13,14] However, such transition-metal oxides and oxynitrides may be not practical catalysts for large-scale solar-energy conversion, because they contain environmentally toxic heavy metals (Pb) or expensive transition metals (Rh, Nb, Ta, or La), which are much less produced than abundant metals such as iron.

Herein, we report that an oxide of abundantly available and environmentally non-toxic tin, Sn_3O_4, can efficiently catalyze the targeted water splitting in aqueous solution under irradiation of visible light. Sn_3O_4 was reported as a first identified mixed-valence tin oxide[15] and has been investigated in terms of the crystal structure.[15−17] Sn_3O_4 belongs to a series of layered tin oxides such as SnO and Sn_2O_3, of which crystal structure consists of stacking of alternating atomic layers of tin and oxygen, but the refined structure of Sn_3O_4 has not been fully elucidated.[17] Recent studies have demonstrated the photoelectric properties[18] and photocatalytic performance of dye degradation of Sn_3O_4,[19] but none has ever shed light to its potential as a photocatalyst for water splitting. We prepared nanocrystals of Sn_3O_4 by hydrothermal synthesis using sodium citrate as a ligand. Scanning electron microscopy (SEM) and transmission electron microscopy (TEM) have shown that the Sn_3O_4 material consisted of thin, highly crystalline flexes (500 × 500 × 10 nm^3), which were predominantly surrounded by the {110} facets. The Sn_3O_4 material was orange in color and more efficiently absorbed visible light than the control SnO_2.

Hydrogen (H_2)-evolution tests in aqueous solution under irradiation of visible light ($\lambda > 400$ nm) have demonstrated that Sn_3O_4 can promote water splitting at a significant efficiency (5 μmol h^{-1}), whereas neither SnO nor SnO_2 is active toward the reaction. Theoretical calculations have elucidated that the

Received: January 8, 2014
Accepted: March 6, 2014
Published: March 10, 2014

   dx.doi.org/10.1021/am500157u | ACS Appl. Mater. Interfaces 2014, 6, 3790−3793

enhanced photocatalytic activity of Sn_3O_4 is attributed to the desirable band structure for photocatalytic H_2 evolution from water solution, which originates from the co-existence of Sn^{2+} and Sn^{4+} in Sn_3O_4: the conduction-band minimum of Sn_3O_4 is higher than the reduction potential for water, and the band gap matches the photon energy of visible light. Sn_3O_4 has great potential as a practical solar-energy conversion catalyst, in terms of low impacts to the environment, abundance of mineral resource, and catalytic performance for the H_2 generation from water solution.

RESULTS AND DISCUSSION

Figure 1a shows the powder X-ray diffraction (*p*XRD) profile for the prepared Sn_3O_4 material (see Experimental Section for the synthetic details). The peak positions and intensities were consistent with the reported *p*XRD pattern for Sn_3O_4, showing the material comprised a single-phase Sn_3O_4 (PDF#20-1293; see the inset for the structural model: $P2_1/c$, a = 0.821 nm, b = 0.493 nm, c = 0.585 nm, β = 94.7°).[16,17] Figure 1b shows the hard X-ray photoemission spectrum (HX-PES) in the Sn 3d region for the Sn_3O_4 material, together with those for metal Sn and SnO_2.[20,21] The Sn $3d_{5/2}$- and $3d_{3/2}$ emissions from the Sn_3O_4 material (486.93±0.20 and 495.33±0.20 eV) are similar in peak positions to the Sn $3d_{5/2}$- and $3d_{3/2}$ emissions from SnO_2 (486.83 ± 0.20 and 495.23 ± 0.20 eV), each of which is 1.9 eV higher than the corresponding emission peaks for Sn (484.95 ± 0.20 and 493.40 ± 0.20 eV). The Sn_3O_4 material contained no zero-valence Sn^0 impurities.

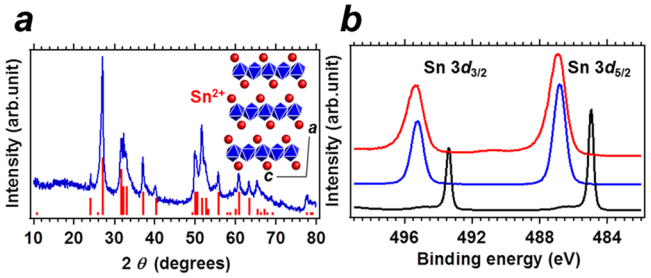

Figure 1. (a) *p*XRD profile for the prepared Sn_3O_4, together with the reported *p*XRD pattern (red bars) and the structural model.[16,17] The red spheres and the blue polyhedra depict the Sn^{2+} cations and the $Sn^{4+}O_6$ octahedra, respectively. (b) HX-PES profiles in the Sn 3d region for Sn (black), SnO_2 (blue), and Sn_3O_4 (red).

Images a and b in Figure 2 show scanning-electron microscope (SEM) images of the Sn_3O_4 material. The Sn_3O_4 material was an aggregate of thin, rectangular flexes with an approximate dimension of 500×500×10 nm^3 (see S5 in the Supporting Information). The sharp reflection spots observed in the selected-area electron diffraction (SAED) pattern, which corresponds to the ⟨110⟩ zone axis of Sn_3O_4 (the inset of Figure 2c), indicate that the individual flexes were single-domain and of high crystallinity. High-resolution TEM observation has also demonstrated that the constituent atoms of the Sn_3O_4 material were highly ordered to form the extremely extended {110} plane (see a structural model as the inset).

Figure 3a shows the absorption spectra of SnO, SnO_2, and Sn_3O_4 in the ultraviolet/visible (UV/vis) region. The SnO material exhibited no distinct structure in the absorption spectrum in the UV/vis range, suggesting that SnO is either a narrow-gap semiconductor or a semimetal. The SnO_2 material had a steep absorption edge in the UV region, corresponding to an interband transition of SnO_2, whereas the Sn_3O_4 material exhibited a broad range of absorption of visible light. From the corresponding extinction spectra (Inset of Figure 3a), we conclude that Sn_3O_4, which is orange in color, has a narrower band gap (2.4 eV) than does the visible-light translucent SnO_2 (3.5 eV).

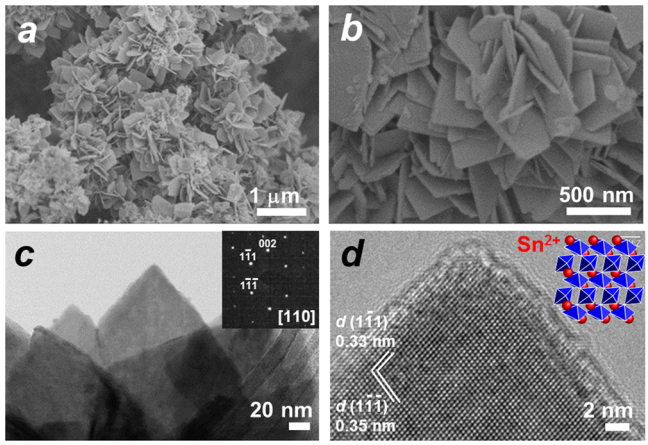

Figure 2. (a,b) SEM and (c,d) TEM images of the Sn_3O_4 material. The insets of (c) and (d) present the corresponding SAED pattern and structural model, respectively. The red spheres and blue polyhedra in the structural model depict the Sn^{2+} cations and the $Sn^{4+}O_6$ octahedra, respectively.

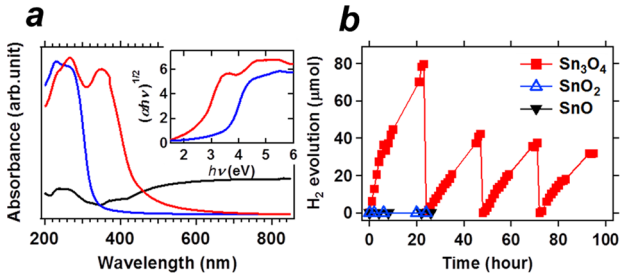

Figure 3. (a) UV–vis absorption spectra of SnO (black), SnO_2 (blue) and Sn_3O_4 (red). The corresponding extinction spectra for SnO_2 and Sn_3O_4 are presented as an inset. (b) Photocatalytic H_2 evolution from the aqueous methanol solution over SnO (black triangles), SnO_2 (blue triangles) and Sn_3O_4 (red squares) with 0.5 wt % Pt loading under the irradiation visible light (300 mg catalyst, λ > 400 nm).

Figure 3b shows the time courses of hydrogen (H_2) evolution over the SnO-, SnO_2-, and Sn_3O_4 materials under irradiation of visible light (λ > 400 nm). Neither the SnO- nor SnO_2 materials exhibited finite H_2 evolution. The Sn_3O_4 material, however, continuously promoted the H_2-evolution over 96 h. Importantly, the H_2 evolution rate in the first 12 h was more than 5 μmol h^{-1}, which is competitive to the performance of reported visible-light-sensitive photocatalysts.[12,22] Moreover, the H_2 evolution rate for the Sn_3O_4 material under irradiation of a Xe lump (UV + visible light, λ > 300 nm) was more than 40 μmol h^{-1} (see Figure S9 in the Supporting Information), whereas neither the SnO- nor SnO_2 materials yielded H_2 . It is worth noting that the Sn_3O_4 material, when containing no Pt co-catalyst, poorly promotes the H_2 evolution under illumination of visible light (see Figure S10 in the Supporting Information). We surmise that the H_2 evolution undergoes over the surface of the Pt co-catalyst and/or at the interface between Pt co-catalyst and Sn_3O_4.

dx.doi.org/10.1021/am500157u | ACS Appl. Mater. Interfaces 2014, 6, 3790–3793

The band edge positions of three kinds of tin oxides are theoretically calculated with respect to those of rutile-type TiO_2 (Figure 4, see also Table S2 in the Supporting Information).[23−25] The reduction potential of water is known to be situated right below the conduction band minimum of TiO_2, and the band alignment shown in Figure 4 is, therefore, useful to understand the capability of tin oxides for H_2 evolution. The calculated band gap of Sn_3O_4 is, as expected from the optical measurements (Figure 3a), in an absorption range of visible light. Note that the reduction potential for water is situated below the conduction band minimum of Sn_3O_4, indicating that this material has great potential for H_2 evolution from water under irradiation of visible light (Figure 3b).

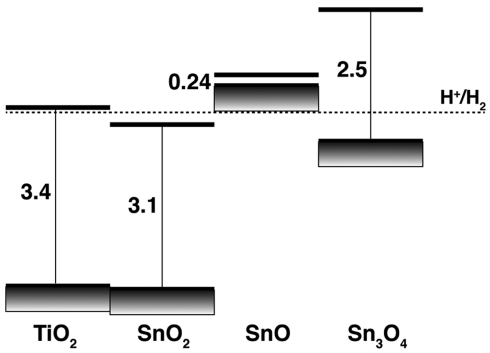

Figure 4. Band alignment of, SnO_2, SnO, and Sn_3O_4, with respect to the band edge positions of rutile-type TiO_2, which are based on the computational calculations on the work functions and band gaps (see Table S1 in Supporting Information). The reduction potential of water is denoted as a horizontal dotted line with a label (H^+/H_2). The band gaps are in eV.

As understood from the calculated local density of states (DOS) for SnO (see Figure S11a in the Supporting Information), in which all the Sn cations are divalent (Sn^{2+}), the occupied band of SnO consists of the Sn s, p states and the O p state, resulting in a very small band gap. By contrast, the valence-band maximum is purely composed of the O p state in SnO_2, of which all the Sn cations are tetravalent (Sn^{4+}), and the band gap is widely opened (see Figure S11b in the Supporting Information). It is clear that the Sn^{2+} cations are responsible for the upshift of the valence-band maximum and the band-gap narrowing in SnO, in comparison to SnO_2 (Figure 4). Unlike either SnO or SnO_2, two different kinds of cation, Sn^{2+} and Sn^{4+}, co-exist in Sn_3O_4 (two Sn^{2+} and one Sn^{4+} per formula unit, see Table S3 in the Supporting Information). The band structure of Sn_3O_4 is expected to be in between those of SnO and SnO_2. This expectation is supported by the calculated local DOS of Sn_3O_4 (see Figures S11c, d in the Supporting Information), which exhibits the appearance of the Sn^{2+}-related states at the top of the valence band while retaining a moderate band gap, 2.5 eV. We also found that the band structure of Sn_3O_4 possesses a great advantage on efficient optical absorption and carrier separation under visible-light irradiation (see Figures S12 and S13 in the Supporting Information). The significant photocatalytic performance of Sn_3O_4 originates from synergetic effects of appropriate band-edge position for H_2 evolution and the desirable band structures for visible light absorption and carrier separation.

CONCLUSION

In conclusion, we have demonstrated that a mixed-valence Sn_3O_4 material, which was prepared by hydrothermal synthesis and characterized with *p*XRD, HX-PES, SEM, and TEM, exhibits significant photocatalytic performance for water splitting under irradiation of visible light (λ > 400 nm), whereas none of the stable tin oxides, SnO and SnO_2, was active toward the reaction. Theoretical calculations have elucidated that the enhanced activity of Sn_3O_4 is attributed to the coexistence of Sn^{2+} and Sn^{4+}, resulting in a desirable band gap and band-edge position for the reduction of water in visible light. The discovery of Sn_3O_4 will prompt the further exploration for visible-light-sensitive photocatalysts composed of abundant, cheap and environmentally benign metal oxides, which will meet the energy/environmental challenges we face.

EXPERIMENTAL SECTION

Synthesis of Sn_3O_4. The Sn_3O_4 material was prepared by a hydrothermal method. $SnCl_2{\cdot}2H_2O$ (0.90 g, 4.0 mmol) and $Na_3C_6H_5O_7{\cdot}2H_2O$ (2.94 g, 10 mmol) were dissolved in 10 mL of Milli-Q water and stirred for 5 min. An aliquot of 10 mL of 0.2 M NaOH aqueous solution was added to the above solution while continuously stirring to obtain a homogeneous solution, which was then transferred to a 40 mL Teflon-lined stainless steel autoclave. After heating in an electric furnace at 180 °C for 12 h, the autoclave was cooled to room temperature. The obtained precipitate was separated by centrifugation and washed several times using Milli-Q water and acetone. Finally, the product was dried under vacuum at room temperature. The yield was 50%.

Photocatalytic Tests. The H_2 evolution experiments were carried out in a gas-closed circulation system. In a typical reaction, the catalyst powder (0.3 g) was dispersed by using a magnetic stirrer in CH_3OH aqueous solution (220 mL of distilled water + 50 mL of CH_3OH) in Pyrex cell with a side window. The 0.5 wt % Pt co-catalyst was photo-deposited on the Sn_3O_4 catalyst by adding a calculated amount of H_2PtCl_6 solution into the reaction solution. The light source was a 300 W of Xe arc lamp with an L42 cut-off filter (λ > 400 nm). The H_2 evolution was measured with an on-line gas chromatograph (GC-8A, Shimadzu) with a thermal conductivity detector (TCD) according to the standard curve.

ASSOCIATED CONTENT

Supporting Information

Materials, characterization (*p*XRD, HX-PES, SEM, and TEM), the results of photocatalytic tests, and computational DOS calculations. This material is available free of charge via the Internet at http://pubs.acs.org/.

AUTHOR INFORMATION

Corresponding Authors

*E-mail: ABE.Hideki@nims.go.jp.
*E-mail: UMEZAWA.Naoto@nims.go.jp.

Notes

The authors declare no competing financial interest.

ACKNOWLEDGMENTS

This work was preliminarily supported by the JST PRESTO program. The HX-PES measurements were performed under the approval of the NIMS Beamline Station (Proposal 2013 B4602). The authors are grateful to HiSOR, Hiroshima

University, and JAEA/SPring-8 for the development of HX-PES at BL15XU of SPring-8.

REFERENCES

(1) Tong, H.; Ouyang, S.; Bi, Y.; Umezawa, N.; Oshikiri, M.; Ye, J. Nano-photocatalytic Materials: Possibilities and Challenges. *Adv. Mater.* **2012**, *24*, 229−251.
(2) Hoffmann, M. R.; Martin, S. T.; Choi, W. Y.; Bahnemann, D. W. Environmental Applications of Semiconductor Photocatalysis. *Chem. Rev.* **1995**, *95*, 69−96.
(3) Osterloh, F. E. Inorganic Materials as Catalysts for Photochemical Splitting of Water. *Chem. Mater.* **2008**, *20*, 35−54.
(4) Zhan, N.; Liu, S.; Xu, Y. J. Recent Progress on Metal Core@ semiconductor Shell Nanocomposites as a Promising type of Photocatalyst. *Nanoscale* **2012**, *4*, 2227−2238.
(5) Zhan, N.; Zhang, Y.; Xu, Y. J. Recent Progress on Graphene-based Photocatalysts: Current Status and Future Perspectives. *Nanoscale* **2012**, *4*, 5792−5813.
(6) Fan, W.; Zhang, Q.; Wang, Y. Semiconductor-based Nanocomposites for Photocatalytic H_2 Production and CO_2 Conversion. *Phys. Chem. Chem. Phys.* **2013**, *15*, 2632−2649.
(7) Chen, X. B.; Shen, S. H.; Guo, L. J.; Mao, S. S. Semiconductor-based Photocatalytic Hydrogen Generation. *Chem. Rev.* **2010**, *110*, 6503−6570.
(8) Kudo, A.; Miseki, Y. Heterogeneous Photocatalyst Materials for Water Splitting. *Chem. Soc. Rev.* **2009**, *38*, 253−278.
(9) Yoshimura, J.; Ebina, Y.; Tanaka, A.; Kondo, J.; Domen, K. Visible Light-induced Photocatalytic Behavior of a Layered Perovskite-type Rubidium Lead Niobate, $RbPb_2Nb_3O_{10}$. *J. Phys. Chem.* **1993**, *97*, 1970−1973.
(10) Hosogi, Y.; Shimodaira, Y.; Kato, H.; Kobayashi, H.; Kudo, A. Role of Sn^{2+} in the Band Structure of SnM_2O_6 and $Sn_2M_2O_7$(M = Nb and Ta) and Their Photocatalytic Properties. *Chem. Mater.* **2008**, *20*, 1299−1307.
(11) Ishii, T.; Kato, H.; Kudo, A. H_2 Evolution from an Aqueous Methanol Solution on $SrTiO_3$ Photocatalysts Codoped with Chromium and Tantalum Ions under Visible Light Irradiation. *J. Photochem. Photobiol. A* **2004**, *163*, 181−186.
(12) Konta, R.; Ishii, T.; Kato, H.; Kudo, A. Photocatalytic Activities of Noble Metal Ion Doped $SrTiO_3$ under Visible Light Irradiation. *J. Phys. Chem. B* . **2004**, *108*, 8992−8995.
(13) Hara, M.; Hitoki, G.; Takata, T.; Kondo, J. N.; Kobayashi, H.; Domen, K. Ta_3N_5 and TaON as Novel Photocatalysts Responding to Visible Light. *Stud. Surf. Sci. Catal.* **2003**, *145*, 169−172.
(14) Kasahara, A.; Nukumizu, K.; Hitoki, G.; Takata, T.; Kondo, J. N.; Hara, M.; Kobayashi, H.; Domen, K. Photoreactions on $LaTiO_2N$ under Visible Light Irradiation. *J. Phys. Chem. A.* **2002**, *106*, 6750−6753.
(15) Lawson, F. Tin Oxide−Sn_3O_4. *Nature* **1967**, *215*, 955−956.
(16) White, T. A.; Moreno, M. S.; Midgley, P. A. Z. Structure Determination of the Intermediate Tin Oxide Sn_3O_4 by Precession Electron Diffraction. *Z. Kristallogr.* **2010**, *225*, 56−66.
(17) Seko, A.; Togo, A.; Oba, F.; Tanaka, I. Structure and Stability of a Homologous Series of Tin Oxides. *Phys. Rev. Lett.* **2008**, *100*, 045702.
(18) Berengue, O.M.; Simon, R. A.; Chiquito, A. J.; Dalmaschio, C. J.; Leite, E. R.; Guerreiro, H. A.; Guimarñaes, F. E. G. Semiconducting Sn_3O_4 Nanobelts: Growth and Electronic Structure. *J. Appl. Phys.* **2010**, *107*, 033717.
(19) He, Y.; Li, D.; Chen, J.; Yu, S.; Xian, J.; Zheng, X.; Wang, P. Sn_3O_4: A Novel Heterovalent-Tin Photocatalyst with Hierarchical 3D Nanostructures under Visible Light. *RSC Adv.* **2014**, *4*, 1266−1269.
(20) Ohsawa, T.; Ohashi, N.; Adachi, Y.; Sakaguchi, I.; Ryoken, H.; Matsumoto, K.; Haneda, H.; Ueda, S.; Yoshikawa, H.; Kobayashi, K. Hard X-ray Photoemission Spectroscopy in Wurtzite-type Zinc Magnesium Oxide Solid-solution Films Grown by Pulsed-laser Deposition. *Appl. Phys. Lett.* **2008**, *92*, 232108.
(21) Ohsawa, T.; Adachi, Y.; Sakaguchi, I.; Matsumoto, K.; Haneda, H.; Ueda, S.; Yoshikawa, H.; Kobayashi, K.; Ohashi, N. Electronic States in Zinc Magnesium Oxide Alloy Semiconductors: Hard X-ray Photoemission Spectroscopy and Density Functional Theory Calculations. *Chem. Mater.* **2009**, *21*, 144−150.
(22) Ouyang, S. X.; Tong, H.; Umezawa, N.; Cao, J. Y.; Li, P.; Bi, Y. P.; Zhang, Y. J.; Ye, J. H. Surface-Alkalinization-Induced Enhancement of Photocatalytic H_2 Evolution over $SrTiO_3$-Based Photocatalysts. *J. Am. Chem. Soc.* **2012**, *134*, 1974−1977.
(23) Heyd, J.; Scuseria, G.; Ernzerhof, M. Hybrid Functionals Based on a Screened Coulomb Potential. *J. Chem. Phys.* **2003**, *118*, 8207−8215.
(24) Kresse, G.; Hafner, J. Ab Initio Molecular-Dynamics for Liquid-Metals. *Phys. Rev. B.* **1993**, *47*, 558−561.
(25) Kresse, G.; Furthmüller, J. Efficient Iterative Schemes for Ab Initio Total-energy Calculations using a Plane-wave Basis Set. *Phys. Rev. B.* **1996**, *54*, 11169−11186.